Different routes towards oscillatory zoning in the growth of solid solutions

Ihor Lubashevsky,[1,2,3,*] Tanja Mues,[1,4,†] and Andreas Heuer[1,4,‡]
[1]*Westfälische Wilhelms Universität Münster, Institut für Physikalische Chemie, Corrensstrasse 30, D-48149 Münster, Germany*
[2]*A.M. Prokhorov General Physics Institute, Russian Academy of Sciences, Vavilov Street 38, 119991 Moscow, Russia*
[3]*Moscow Technical University of Radioengineering, Electronics, and Automation, Vernadsky 78, 119454 Moscow, Russia*
[4]*Center of Nonlinear Science CeNoS, Westfälische Wilhelms Universität Münster, D-48149 Münster, Germany*
(Received 29 May 2008; published 16 October 2008)

Oscillatory zoning, i.e., self-formation of spatial quasiperiodic oscillations in the composition of solid growing from aqueous solution, is analyzed theoretically. Keeping in mind systems like $(Ba,Sr)SO_4$, we propose a one-dimensional model that takes into account the nonideality of the solid solution and the system asymmetry, in particular, reflecting itself in different solubilities for such systems. Based on a linear stability analysis, different parameter regions can be identified. Even an ideal solution with a sufficiently large asymmetry can display oscillatory zoning. Numerical simulations complement the linear stability analysis as well as the qualitative consideration of the instability development and reveal the nature of the limit cycles.

DOI: 10.1103/PhysRevE.78.041606 PACS number(s): 81.10.Aj, 47.54.−r, 05.65.+b, 82.40.Ck

I. INTRODUCTION

Spatial patterns reflected by quasiperiodic variations of the solid composition from the core of crystals to their rim are widely met in natural minerals (see, e.g., Ref. [1]). This phenomenon is called oscillatory zoning (OZ). The appearance of such patterns was traditionally related to cyclic changes in surroundings during crystal formation in rocks. However, the success of reproducing OZ in calcite crystals [2] and $(Ba,Sr)SO_4$ solid solutions [3–5] in laboratory under quasistationary conditions has demonstrated that OZ can at least partly result from self-organization during crystal growth in solution.

The experimental setup used by Putnis and co-workers [3–5] is sketched in Fig. 1. It consists of two reservoirs, one filled with an aqueous solution of $BaCl_2/SrCl_2$ and the other with Na_2SO_4. The two reservoirs are connected by a column filled with silica gel to inhibit convective transport. At the beginning of the experiments the reactants start to diffuse toward each other through the column. As the diffusion fields of Ba^{2+}, Sr^{2+}, and SO_4^{2-} overlap and the solute concentration product exceeds the nucleation threshold in the vicinity of the column center, the crystal nuclei form. In approximately one month the experiments were terminated. The obtained crystals exhibited OZ although no external fluctuations were imposed on the system.

Following the spirit of the general model by Ortoleva [6,7] for the growth instability caused by autocatalytic interaction of the species at the crystal surface L'Heureux *et al.* [8–10] proposed a rather sophisticated model for OZ in the $(Ba,Sr)SO_4$ solid growing from aqueous solution. The detailed analysis of these models was carried out within the boundary layer approximation.

In a previous paper [11] we have demonstrated that OZ in crystals growing from solution can be described as a boundary-reaction-diffusion problem. It is characterized by passive diffusion of species through the solution bulk to the crystal surface where their interaction gives rise to the crystal growth. The latter, however, proceeds with a very low rate so that the crystal boundary can be treated as a surface fixed in space. In that work we have mainly studied the presence of the instability with respect to the nonideality parameter θ. It turned out that for sufficiently large θ, i.e., $\theta > \theta_{c0}$ the instability and thus OZ can indeed be observed.

Experimentally, however, it is observed that in particular solid solutions with very different solubility products of the end members display OZ [such as $(Ba,Sr)SO_4$] whereas systems with similar solubility products [such as $(Ba,Sr)CO_3$] do not display OZ [12]. For example, for the first case the solubility product of both end members differs by three orders of magnitude (see, e.g., [13]). The solubility product is related to the system asymmetry ϕ. Thus the question emerges whether the model also allows OZ for systems with a pronounced asymmetry rather than a significant nonideality.

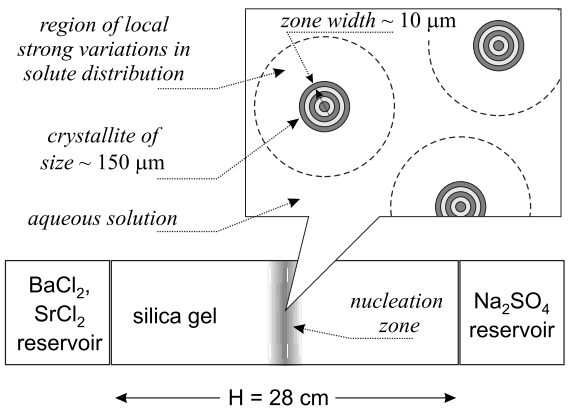

FIG. 1. Experimental setup in which oscillatory zoned crystals of $(Ba,Sr)SO_4$ were synthesized by Putnis and co-workers [3–5]. The reactants counterdiffuse in the column and $(Ba,Sr)SO_4$ crystals nucleate. The upper window sketches the structure of the nucleation zone and the length scales involved.

*ialub@fpl.gpi.ru
†t_mues01@uni-muenster.de
‡andheuer@uni-muenster.de

The purpose of this work is fourfold. First, we rederive our model in a somewhat extended way which allows one to better understand the microscopic origin of the different parameters. The definitions have been chosen such that the final model equations are identical to the model studied in our previous work [11]. Second, after deriving the somewhat complex instability conditions from the linear stability analysis we argue on a semiquantitative level that indeed the model possesses an additional instability channel for sufficiently large values of the system asymmetry and thus obtain a semiquantitative phase diagram of the instability region. Third, via a careful mathematical analysis, we somewhat modify this picture, yielding some surprising features in the newly analyzed instability regime. Fourth, via numerical simulations we illustrate the behavior beyond the linear regime.

II. MODEL

A. Energetics of crystal growth

We take into account the following mechanism of crystal growth having in mind the $(Ba,Sr)SO_4$. The ions SO_4^{2-} (below species of type 0), Ba^{2+} (species 1), and Sr^{2+} (species 2) diffuse to the crystal surface through the aqueous solution, where they are adsorbed and display surface diffusion. If they reach the atomic steps they are incorporated into the crystalline lattice via the following precipitation reactions:

$$Ba^{2+} + SO_4^{2-} \rightarrow BaSO_4 \quad \text{(channel 0-1)}, \tag{1a}$$

$$Sr^{2+} + SO_4^{2-} \rightarrow SrSO_4 \quad \text{(channel 0-2)}. \tag{1b}$$

The latter process is considered to be irreversible, i.e., the solid dissolution is ignored, which means that the system is far from thermal equilibrium and the growth rate cannot take too low values in the case under consideration. Finally, they are forming a new layer of the crystal.

Migrating along the crystal surface adatoms experience many different local environments depending on the surface composition which will be characterized by the mole fraction χ of species 1 $(0 \leqslant \chi \leqslant 1)$. The competition between adsorption and desorption is determined by the effective adsorption energies $E_i(\chi)$ $(i=0,1,2)$ reflecting the species interaction with the crystal surface and aqueous solvent. In the mean field approximation they are written as

$$E_0(\chi) = \epsilon_0 - g_1\chi - g_2(1-\chi), \tag{2a}$$

$$E_1(\chi) = \epsilon_1 - g_1 + \theta(1-\chi), \tag{2b}$$

$$E_2(\chi) = \epsilon_2 - g_2 + \theta\chi, \tag{2c}$$

where all the energy quantities are measured in units of temperature. Here ϵ_i is the solvation energy of species i, the constant g_i characterizes the interaction between adatoms of type $i=1,2$ with atoms of type 0 lying in the surface atomic layer of the crystal lattice, and the parameter $\theta > 0$ quantifies the solid solution nonideality. This expresses the fact that the strongest interaction on the crystal surface holds between like ions.

In these terms equilibrium between the adsorbed layer and the aqueous solution region adjacent to the crystal surface implies the following relation between the adatom concentrations c_i and the concentration C_i^s of the corresponding species near the crystal surface:

$$c_i = aC_i^s e^{-E_i(\chi)}, \tag{3}$$

where a is the characteristic size of the crystalline cell.

In principle, on vicinal crystal surfaces the adatoms should have some solvent shells and for them to be incorporated into the crystal lattice these shells have to be destroyed. If it is essential then the precipitation reactions (1) at the surface atomic steps limit the crystal growth and it can be assumed that the absorbed layer is in quasiequilibrium as expressed by Eq. (3). In this case the partial rates ϑ_1 and ϑ_2 of the crystal growth through channels (1a) and (1b), i.e., the individual contributions of these channels to the interface velocity of the growing crystal are given by the expression

$$\vartheta_i = \nu_i \frac{a^6}{l} c_0 c_i, \tag{4}$$

where ν_i is the frequency at which the pair of the Ba^{2+}, SO_4^{2-} adatoms or the Sr^{2+}, SO_4^{2-} adatoms meeting at the surface steps are incorporated in the crystal lattice and l is the mean distance between these steps.

Combining expressions (3) and (4) we get the desired relationship between the partial growth rates via the channels 0-1, 0-2, and the corresponding values of the solute concentrations C_0^s, C_1^s, and C_2^s near the crystal surface,

$$\vartheta_1 = \varpi \left(\frac{\nu_1}{\nu_2}\right)^{1/2} e^{-(1/2)\eta} e^{\phi\chi - \theta(1-\chi)} C_0^s C_1^s, \tag{5a}$$

$$\vartheta_2 = \varpi \left(\frac{\nu_2}{\nu_1}\right)^{1/2} e^{(1/2)\eta} e^{-\phi(1-\chi) - \theta\chi} C_0^s C_2^s. \tag{5b}$$

Here we have introduced the kinetic coefficient

$$\varpi = \sqrt{\nu_1 \nu_2} \frac{a^8}{l} e^{2g_{12} - \epsilon_0 - \epsilon_{12}} \tag{6}$$

and rewritten the interaction constants $g_{1,2}$, $\epsilon_{1,2}$ using combination of the quantities

$$g_{12} = \frac{1}{2}(g_1 + g_2), \quad \phi = g_1 - g_2, \tag{7}$$

$$\epsilon_{12} = \frac{1}{2}(\epsilon_1 + \epsilon_2), \quad \eta = \epsilon_1 - \epsilon_2 \tag{8}$$

to emphasize the different properties of species 1 and 2.

Expressions (5) are actually the main result of this subsection and form the basis of the model for the crystal growth to be constructed in the next section. It is rather similar to the model we have developed previously [11], enabling us to sketch out the principle aspects only. Below we will assume the inequality $\phi > 0$ to hold beforehand because, otherwise, the indices could just be exchanged.

B. Model equations

In the aqueous solution the SO_4^{2-} ions are assumed to be abundant. Thus we can regard their concentration as a fixed value C_0. In this case the crystal growth in the one-dimensional (1D) description is governed by the boundary-reaction-diffusion model developed in our previous work [11]. Namely, diffusion of the components $i=1,2$ through the solution is considered within the region $z\in[0,L]$ and is described by the equation

$$\frac{\partial C_i(z,t)}{\partial t} = D_i \frac{\partial^2 C_i(z,t)}{\partial z^2}, \tag{9}$$

where D_i is the diffusivity of the species i in the aqueous solution and the system size L should be chosen large enough in order to enable us to fix the influx of both the components at the external boundary $z=L$

$$G_i = D_i \left.\frac{\partial C_i(z,t)}{\partial z}\right|_{z=L}. \tag{10}$$

Then having in mind expressions (5) we write the following boundary condition at the crystal surface ($z=0$):

$$D_i \left.\frac{\partial C_i(z,t)}{\partial z}\right|_{z=0} = \frac{aC_i^s}{\tau_i(\chi)} \tag{11}$$

which relates the boundary values of diffusion flux and the rates of species attachment to the crystal surface,

$$r_i := \frac{aC_i^s}{\tau_i(\chi)}, \tag{12}$$

caused by the growth process. Here the time scales of the crystal growth dynamics via the channels 0-1 and 0-2 individually are specified as

$$\tau_1(\chi) = \tau_g \left(\frac{\nu_2}{\nu_1}\right)^{1/2} e^{(1/2)\eta - \phi\chi + \theta(1-\chi)}, \tag{13a}$$

$$\tau_2(\chi) = \tau_g \left(\frac{\nu_1}{\nu_2}\right)^{1/2} e^{-(1/2)\eta + \phi(1-\chi) + \theta\chi}, \tag{13b}$$

where the time scale of the crystal growth dynamics as a whole process is

$$\tau_g = \frac{a^4}{\varpi C_0}. \tag{14}$$

Finally, the solid composition is governed by the equation

$$\frac{d\chi}{dt} = a^2 \left((1-\chi)\frac{aC_1^s}{\tau_1(\chi)} - \chi\frac{aC_2^s}{\tau_2(\chi)}\right) \tag{15}$$

following from mass conservation and used previously in a number of papers on OZ; see, e.g., Refs. [8–11].

The given system admits only one steady state solution,

$$C_1(z) = C_{1,\mathrm{st}}^s + \chi_{\mathrm{st}}\frac{G}{D_1}z,$$

$$C_2(z) = C_{2,\mathrm{st}}^s + (1-\chi_{\mathrm{st}})\frac{G}{D_2}z, \tag{16a}$$

where $G=G_1+G_2$ is the total diffusion flux determining the growth rate of the crystal as a whole, the corresponding value of the crystal composition $\chi_{\mathrm{st}}=G_1/G$, so

$$G_1 = \chi_{\mathrm{st}}G, \quad G_2 = (1-\chi_{\mathrm{st}})G, \tag{16b}$$

and by virtue of Eq. (11) the boundary values of the species concentrations are

$$C_{1,\mathrm{st}}^s = \frac{\tau_1(\chi_{\mathrm{st}})}{a}\chi_{\mathrm{st}}G,$$

$$C_{2,\mathrm{st}}^s = \frac{\tau_2(\chi_{\mathrm{st}})}{a}(1-\chi_{\mathrm{st}})G. \tag{16c}$$

It should be noted that this model contains as variables the solid state composition χ and two boundary values of the species concentrations C_1^s, C_2^s. So the system instability can be described using the classical notions of relaxation oscillations in a two-dimensional phase plane. This, however, is only a rough approximation, as it has been already shown in our previous paper [11].

III. THE INSTABILITY DOMAIN

A. The eigenvalue problem

Now let us analyze in a rigorous way the linear stability of the system around the steady state described by expressions (16a)–(16c). For this purpose the dynamics of small perturbations

$$\delta C_i(t,z) \propto \exp\{\gamma t - p_i z\}, \quad \delta\chi(t) \propto \exp\{\gamma t\} \tag{17}$$

in the species distribution and the composition of the crystal surface is considered. Here γ is the instability increment and the parameters $\{p_i\}$ such that $\mathrm{Re}\, p_i > 0$ characterize localization of the perturbations $\delta C_i(t,z)$ near the crystal surface. Then the governing equations (9)–(11) and (15) are linearized with respect to perturbations (17) in the vicinity of the stationary solution (16a)–(16c). The system of algebraic equations obtained in this way gives us the eigenvalue equation for the instability increment γ. This procedure is practically identical to that from Ref. [11]. So here we skip the corresponding mathematical manipulations and write directly the desired eigenvalue equation in the final form,

$$\frac{\zeta^2}{g}e^{i2\psi} = -1 + \chi(1-\chi)\left[(\theta+\phi)\frac{(\zeta\Delta)e^{i\psi}}{(\zeta\Delta)e^{i\psi}+1} + (\theta-\phi)\frac{(\zeta/\Delta)e^{i\psi}}{(\zeta/\Delta)e^{i\psi}+1}\right], \tag{18}$$

where following the notations of paper [11] we have introduced the variable $\zeta>0$, the angle $\psi\in(-\pi/2,\pi/2)$, and the parameter $\Delta>0$ given by the expression

$$\Delta^2 = \sqrt{\frac{D_1}{D_2}}\frac{\tau_1(\chi)}{\tau_2(\chi)} = \Delta_\phi^2 \exp\{\theta(1-2\chi)\}$$

$$\text{with } \Delta_\phi^2 = \sqrt{\frac{D_1}{D_2}}\frac{\nu_2}{\nu_1}\exp\{\eta-\phi\} \tag{19}$$

such that

$$\gamma = \frac{a^2}{\sqrt{D_1 D_2}\tau_1(\chi)\tau_2(\chi)}\zeta^2 e^{i2\psi}, \tag{20}$$

and

$$p_1 = \frac{a}{D_1\tau_1(\chi)}\Delta\zeta e^{i\psi}, \quad p_2 = \frac{a}{D_2\tau_2(\chi)}\frac{1}{\Delta}\zeta e^{i\psi}. \tag{21}$$

The quantity g stands for the dimensionless diffusion flux of species through the aqueous solution bulk towards the crystal surface,

$$g = \sqrt{D_1 D_2}\tau_1(\chi)\tau_2(\chi)G = \sqrt{D_1 D_2}\tau_g^2 \exp\{\phi(1-2\chi)+\theta\}G. \tag{22}$$

To find the boundary of the instability region in the space of system parameters we note that the eigenvalue equation (18) can be directly reduced to a fourth-order polynomial equation by multiplying it by both the denominators entering its right-hand side. The coefficient of the highest power term of this polynomial is a constant value. So the roots of Eq. (18) cannot go to infinity and thus vary continuously as the system parameters change. The instability boundary separates the regions where the value of Re γ has different signs and therefore meets the equality

$$\text{Re } \gamma = 0.$$

Due to Eq. (20) this converts into the condition $\psi = \pm\pi/4$. Taking the latter into account and splitting Eq. (18) into the real and imaginary parts we immediately get the conclusion that at the instability boundary the parameter ζ obeys the following equation:

$$(\theta+\phi)\Psi_1(\zeta\Delta) + (\theta-\phi)\Psi_1\left(\frac{\zeta}{\Delta}\right) = 2\Theta_c \tag{23}$$

and the diffusion flux takes the value

$$g_c = \sqrt{2}\Theta_c\zeta_c\left[(\theta+\phi)\Delta\Psi_2(\zeta_c\Delta) + (\theta-\phi)\frac{1}{\Delta}\Psi_2\left(\frac{\zeta_c}{\Delta}\right)\right]^{-1}, \tag{24}$$

where ζ_c is the solution of Eq. (23) and the functions

$$\Psi_1(x) = \frac{\sqrt{2}x(\sqrt{2}x+1)}{(\sqrt{2}x+1)^2+1}, \quad \Psi_2(x) = \frac{1}{(\sqrt{2}x+1)^2+1} \tag{25}$$

as well as the critical value of the nonideality parameter depending on the crystal composition χ,

$$\Theta_c(\chi) = \frac{1}{2\chi(1-\chi)}, \tag{26}$$

have been introduced. In other words, at the instability boundary the general eigenvalue equation (18) is reduced to Eq. (23) and if its solution ζ_c exists then formula (24) specifies the critical value of the species diffusion flux g_c. Only one additional condition should be imposed; it is the requirement that the obtained value of g_c be positive.

Below we will confine our consideration to the case $\chi = 0.5$ only for which $\Theta_c := \theta_{c0} = 2$. Indeed, first, this value of the solid composition χ determines precisely the actual boundaries, external and internal ones, of the instability regions to be analyzed. Second, as follows directly from expressions (23) and (24), by the transformations

$$\theta_{\text{new}} = \theta_{\text{old}}\frac{\Theta_c}{\theta_{c0}}, \quad \phi_{\text{new}} = \phi_{\text{old}}\frac{\Theta_c}{\theta_{c0}} \tag{27}$$

the case of $\chi \neq 0.5$ is reduced immediately to the given one. Naturally the dependence of the system characteristics on the solid composition χ endows the growth instabilities with nontrivial properties. In particular, in some sense "optimal" conditions for the onset of instability can match the solid composition deviating substantially from $\chi = 0.5$, which in turn is able to cause a system instability with respect to spatially nonuniform perturbations. This question, however, is beyond the scope of the present paper. Third, in the mathematical expressions to be obtained below the quantity θ_{c0} will be kept instead of being replaced by its numerical value, so using transformations (27) the general expressions can be reconstructed immediately.

The solution of the system (23) and (24) implicitly determines the critical value $g_c(\theta, \phi, \Delta)$ of the species diffusion flux. Thereby it describes the boundary of the instability region in the complete space of the system parameters $\{g, \theta, \phi, \Delta\}$. Projecting this region onto various planes makes it possible to regard the instability boundary as some curve (or surface) dividing a given plane into two domains, where the instability can arise in principle for a given values of the corresponding parameters or cannot do it at all. Below in this section we will consider in detail this projection onto the plane $\{\theta, \phi\}$ for a fixed value of the parameter Δ with the main attention paid to the limit $\Delta \gg 1$.

It is worthwhile to underline once more that the parameter Δ primarily quantifies the effect of the difference in the solution energies of the species, although its specific value depends also on the difference in their interaction potentials. So the parameters Δ and ϕ complementarily describe the effect of system asymmetry on the crystal growth.

B. Two instability mechanisms

Possible roots $\{\zeta_c\}$ of Eq. (23) specify the eigenvalues determining the critical value of the diffusion flux g_c via expression (24). The instability boundary is the locus where the potentials ϕ and θ take such values that the left-hand side of Eq. (23) gets its maximum at these roots. The solid nonideality and the system asymmetry are responsible for the terms in this equation exhibiting different behavior. The term proportional to θ is an increasing function of ζ, whereas the term proportional to ϕ comprises increasing and decreasing branches. It is the mathematical reflection of different instability mechanisms caused by the solid nonideality and the system asymmetry.

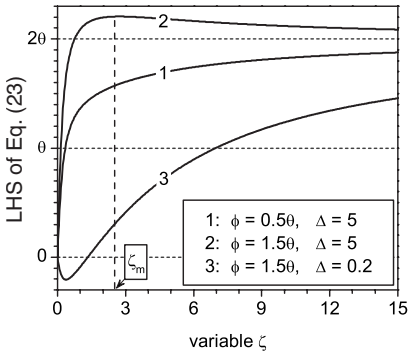

FIG. 2. Left-hand side (LHS) of Eq. (23) as a function of the variable ζ. Curve 1 depicts this dependence when the system asymmetry cannot affect the onset of instability crucially ($\phi < \theta$), curve 2 exhibits the case where the asymmetry effect is pronounced ($\phi > \theta$). Curve 3 demonstrates the fact that the system asymmetry depresses the onset of instability when $\phi > \theta$ and $\Delta < 1$.

The asymmetry effect becomes crucial when the left-hand side of Eq. (23) changes its behavior as a function of ζ. It converts from a function monotonically increasing from 0 to 2θ when ζ runs from 0 to ∞ (curve 1 in Fig. 2) to one possessing a maximum Ψ_m attained at a certain internal point $0 < \zeta_m < \infty$ (curve 2 in Fig. 2). For $0 < \zeta < \zeta_m$ it grows from 0 to $\Psi_m > 2\theta$ and then drops down to 2θ on the interval $\zeta_m < \zeta < \infty$. The asymptotics of the left-hand side of Eq. (23) as $\zeta \to \infty$ demonstrates directly that it is the case when

$$\left(\frac{\phi - \theta}{\phi + \theta}\right)\Delta^2 > 1. \tag{28}$$

In fact, if inequality (28) holds the asymptotics of the left-hand side of Eq. (23) is a decreasing function of ζ and thus the point $0 < \zeta_m < \infty$ does exist. Exactly in this case the instability can arise even the nonideality potential is less than its threshold, $\theta < \theta_{c0}$ provided the maximum $\Psi_m > 2\theta_{c0}$ due to the effect of the system asymmetry. For the latter to be the case the inequality $\Delta > 1$ is necessary as follows from condition (28). For $\Delta < 1$ the system asymmetry depresses the instability onset as it is illustrated in Fig. 2 by curve 3.

Before passing to a detailed analysis of the instability domain we present a fairly simple way to construct the instability boundary in the plane $\{\theta, \phi\}$ for a fixed value of Δ. It applies to the fact that the given system admits two scenarios of the onset of instability. One caused by the solid nonideality matches the eigenvalues $\zeta e^{i\psi} \to \infty$ with the diffusion flux $g \to \infty$. In this case the solution of the general eigenvalue equation (18) can be written as

$$\zeta^2 e^{i2\psi} = g\left(\frac{\theta}{\theta_{c0}} - 1\right) \quad \text{for } g \to \infty, \tag{29}$$

so the instability arises when the nonideality parameter exceeds its critical value, $\theta > \theta_{c0}$, because $\gamma \propto \zeta^2 e^{i2\psi}$. The other is characterized by the bounded variations of the eigenvalues $\zeta e^{i\psi}$ as the diffusion flux goes to infinity. Under this condition we can analyze directly the eigenvalue problem in the limit $g \to \infty$ setting the left-hand side of Eq. (18) equal to zero and thus reducing it actually to a quadratic equation.

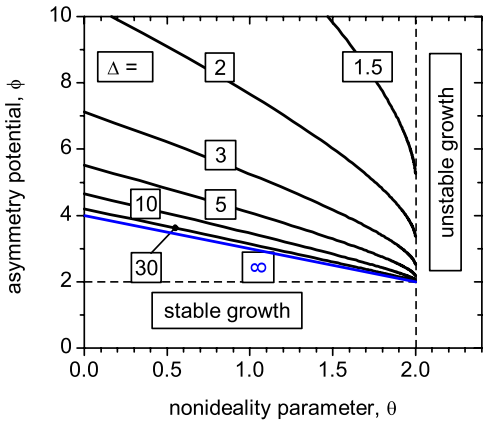

FIG. 3. (Color online) The instability boundary $\mathcal{B}_\phi^+$ for several values of the parameter Δ including the limit value $\Delta = \infty$. The used criterion of instability is Re $\gamma > 0$ for $g \to \infty$.

Omitting simple arithmetical manipulations the result is

$$\zeta e^{i\psi} = \frac{1}{4(\theta_{c0} - \theta)}[\kappa \pm \sqrt{\kappa^2 - 16\theta_{c0}(\theta_{c0} - \theta)}], \tag{30}$$

where

$$\kappa := \left(\Delta + \frac{1}{\Delta}\right)\theta + \left(\Delta - \frac{1}{\Delta}\right)\phi - 2\left(\Delta + \frac{1}{\Delta}\right)\theta_{c0}. \tag{31}$$

For $\theta > \theta_{c0}$ one of these roots corresponds to unstable perturbations, nevertheless, the perturbations matching the eigenvalues given by expression (29) are dominant due to large values of their increments. However, when the solid nonideality is not to high, i.e., $\theta < \theta_{c0}$, the latter perturbations turn out to be stable and the growth instability is caused by the system asymmetry. Indeed, the instability boundary with $\psi = \pm \pi/4$ meets the condition

$$\kappa > 0 \quad \text{and} \quad \kappa^2 = 8\theta_{c0}(\theta_{c0} - \theta). \tag{32}$$

By virtue of Eq. (32) such instability can arise when the parameters ϕ and $\Delta > 1$ reflecting the system asymmetry meet the inequality

$$\phi > \phi_c^+ = \frac{\Delta^2 + 1}{\Delta^2 - 1}(2\theta_{c0} - \theta) + \frac{2\sqrt{2}\Delta}{\Delta^2 - 1}\sqrt{\theta_{c0}(\theta_{c0} - \theta)}. \tag{33}$$

When $\Delta < 1$ the system asymmetry suppresses the instability as noted above in Fig. 2. The curve $\mathcal{B}_\phi^+$ on the plane $\{\theta, \phi\}$ specified by the dependence $\phi_c^+(\theta)$ is presented in Fig. 3 for several values of the parameter Δ. Roughly speaking $\mathcal{B}_\phi^+$ is the boundary of the instability domain for $\theta < \theta_{c0}$.

It should be underlined that the present analysis was based on the assumption that the instability has to arise for large values of the species diffusion flux if it can develop in principle for given values of the other system parameters. It is true when the growth instability is caused by the solid nonideality. However, for the instability induced by the system asymmetry the situation is more intricate. Rigorously speaking, in the latter case at the real instability boundary $\mathcal{B}_\phi$ the species diffusion flux g takes a certain finite value $g_c < \infty$ and in a narrow boundary layer inside the instability

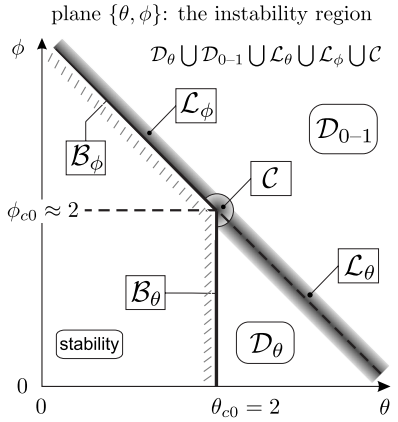

FIG. 4. The structure of the instability region as a whole on the plane $\{\theta,\phi\}$ for a fixed value of the parameter $\Delta \gg 1$. It comprises five regions distinguishable in properties: two volumetric domains $\mathcal{D}_\theta$ and $\mathcal{D}_{0\text{-}1}$, one intermediate layer $\mathcal{L}_\theta$ between them and one boundary layer $\mathcal{L}_\phi$ whose thickness $W_c \gtrsim 1/\Delta \ll 1$, and, finally, a double criticality neighborhood $\mathcal{C}$ of the point $\{\theta_{c0}, \phi_{c0} \approx \theta_{c0}\}$.

region the diffusion flux must belong to a finite interval, $g_c < g < g_c^+ < \infty$. Nevertheless, as will be seen below, this feature is valid only for $\Delta \gtrsim 1$. So as stems from expression (33) for $\Delta \gg 1$ the boundary of the growth instability caused by the system asymmetry is approximated by the line

$$\phi = 2\theta_{c0} - \theta \tag{34}$$

to the leading order in $1/\Delta$.

IV. STRUCTURE OF THE INSTABILITY DOMAIN

Based on the analysis of the eigenvalue equation (23) for $\Delta \gg 1$ we can single out five characteristic regions of the system instability on the plane $\{\theta,\phi\}$ shown in Fig. 4. Let us consider them individually assuming $\Delta \gg 1$ to hold.

A. Instability domain $\mathcal{D}_\theta$

The volumetric domain $\mathcal{D}_\theta$ matches actually the growth instability studied in our previous paper [11]. It is bounded by the vertical line $\mathcal{B}_\theta = \{\theta, \phi: \theta = \theta_{c0} = 2\}$, by the layer $\mathcal{L}_\theta$, and the θ axis. The layer $\mathcal{L}_\theta$ is a certain neighborhood of the line $\phi = 2\theta_{c0} - \theta$ whose thickness is about $W_c \gtrsim 1/\Delta$. In domain $\mathcal{D}_\theta$ condition (28) is strongly violated, i.e.,

$$\left(\frac{\theta - \phi}{\phi + \theta}\right)\Delta^2 \gg 1. \tag{35}$$

So the left-hand side of Eq. (23) is a monotonically increasing function of ζ. Besides, for any point of the domain $\mathcal{D}_\theta$ the distance between it and the line $\phi = 2\theta_{c0} - \theta$, i.e., actually between it and the layer $\mathcal{L}_\theta$, can be regarded as a large value in comparison with the quantity $1/\Delta$. The latter statement, as can be shown directly, causes the solution of Eq. (23) to meet the inequality $\zeta_c \gg 1$. Thereby the former term on the left-hand side of Eq. (23) can be taken in the limit $\zeta\Delta \to \infty$. Also the corresponding term in expression (24) can be ignored. Under these conditions Eq. (23) is reduced to a quadratic equation with respect to ζ, yielding us immediately its solution in the form

$$\zeta_c = \frac{\Delta}{\sqrt{2}} F(r_\theta). \tag{36}$$

Here, by definition, the function $F(r_\theta)$ is determined by the expression

$$F(x) = \frac{1}{2(1-x)}[2x - 1 + \sqrt{1 + 4x(1-x)}]; \tag{37}$$

its argument is

$$r_\theta = \frac{2\theta_{c0} - \theta - \phi}{\theta - \phi} \equiv 1 - \frac{2}{(\theta - \phi)}[\theta - \theta_{c0}]. \tag{38}$$

The inequality $\theta_{c0} < \theta$ is assumed to hold, thus $0 < r_\theta < 1$. Then the critical value g_c of the dimensionless diffusion flux is

$$g_{c\{\mathcal{D}_\theta\}} = \frac{\Delta^2 \theta_{c0}}{(\theta - \phi)} \frac{F^2(r_\theta)[F(r_\theta) + 1]}{r_\theta} \tag{39}$$

by virtue of Eq. (24).

Near the threshold of the nonideality coefficient, i.e., in the vicinity of the boundary $\mathcal{B}_\theta$, where

$$0 < \theta - \theta_{c0} \ll \theta - \phi, \tag{40}$$

one has $1 - r_\theta \ll 1$. In this case function (37) is approximated as $F(r_\theta) \approx 1/(1 - r_\theta)$ and expression (39) is reduced to

$$g_{c\{\mathcal{D}_\theta|\mathcal{B}_\theta\}} \approx \frac{\Delta^2 \theta_{c0}(\theta - \phi)^2}{8(\theta - \theta_{c0})^3}, \tag{41}$$

whence it follows, in particular, that the critical value of diffusion flux diverges as $(\theta - \theta_{c0})^{-3}$ for $\theta \to \theta_{c0} + 0$, being in agreement with the results of paper [11].

When the analyzed point $\{\theta,\phi\}$ is located in a close proximity to the layer $\mathcal{L}_\theta$, i.e., for

$$\frac{1}{\Delta} \ll 2\theta_{c0} - \theta - \phi \ll \theta - \phi \tag{42}$$

one has $r_\theta \ll 1$ and $F(r_\theta) \approx 2r_\theta$. In this case formula (39) is simplified as

$$g_{c\{\mathcal{D}_\theta|\mathcal{L}_\theta\}} \approx \frac{4\Delta^2 \theta_{c0}(2\theta_{c0} - \theta - \phi)}{(\theta - \phi)^2}. \tag{43}$$

We remind that in expression (43) the difference $(2\Theta_c - \theta - \phi)$ cannot become too small according to inequality (42). The behavior of the critical diffusion flux for points coming close to the line $\phi = 2\theta_{c0} - \theta$ is considered below.

B. Instability domain $\mathcal{D}_{0\text{-}1}$

The other volumetric domain $\mathcal{D}_{0\text{-}1}$ of system instability is formally the half plane bounded from below by the layer composition $\mathcal{L}_\theta \cup \mathcal{L}_\phi$, i.e., by a neighborhood of the line $\phi = 2\theta_{c0} - \theta$ with thickness $W_c \gtrsim 1/\Delta$ (Fig. 4). It comprises all the points $\{\theta,\eta\}$ such that

$$\theta + \phi - 2\theta_{c0} \gg \frac{1}{\Delta}. \tag{44}$$

In this region the solution ζ_c of Eq. (23) turns out to be much less than unity, $\zeta_c \ll 1$. As can be verified directly, the latter inequality enables us to ignore both the second terms on the left-hand side of Eq. (23) and inside the square brackets in Eq. (24). The appearance of these terms is due to the channel 0-2 of the precipitation reactions (1). Therefore in the domain $\mathcal{D}_{0\text{-}1}$ the contribution of the channel 0-2 is of minor importance and the growth instability is caused by the channel 0-1 individually.

Using this simplification the eigenvalue equation (23) again can be reduced to a quadratic equation with the solution

$$\zeta_c = \frac{1}{\sqrt{2}\Delta} F(r_{01}), \tag{45}$$

where, by definition, the argument r_{01} is the value

$$r_{01} = \frac{2\theta_{c0}}{\theta + \phi} \tag{46}$$

and meets the inequality $1 - r_{01} \gg 1/\Delta$.

The corresponding expression for the critical value of the species diffusion flux is

$$g_{c\{\mathcal{D}_{0\text{-}1}\}} = \frac{1}{\Delta^2} F^2(r_{01})[F(r_{01}) + 1]. \tag{47}$$

In particular, near the domain boundary $\mathcal{L}_\theta \cup \mathcal{L}_\phi$, i.e., for

$$\frac{1}{\Delta} \lesssim \theta + \phi - 2\theta_{c0} \ll 1, \tag{48}$$

where $1 - r_{01} \ll 1$ and the function $F(r_{01}) \approx 1/(1 - r_{01})$ expression (47) converts into

$$g_{c\{\mathcal{D}_{0\text{-}1}|\mathcal{L}_\theta \cup \mathcal{L}_\phi\}} \approx \frac{8\theta_{c0}^3}{\Delta^2(\theta + \phi - 2\theta_{c0})^3}. \tag{49}$$

It should be pointed out that expression (49) does not describe a real singularity in the diffusion flux threshold. In fact, the difference

$$\sigma := \theta + \phi - 2\theta_{c0} \tag{50}$$

is bounded from below in the domain $\mathcal{D}_{0\text{-}1}$, namely, $\sigma \gg 1/\Delta$ and the limit $\sigma \to +0$ cannot be implemented in it.

By virtue of expression (47) in the domain $\mathcal{D}_{0\text{-}1}$ the diffusion flux threshold g_c practically does not depend on the particular value of the difference $(\theta - \phi)$ because of the minor effect of channel 0-2. The situation changes dramatically when the analyzed point $\{\theta, \phi\}$ enters the boundary of this domain, being the subject of the following subsections.

C. Intermediate layer $\mathcal{L}_\theta$

The instability domains $\mathcal{D}_\theta$ and $\mathcal{D}_{0\text{-}1}$ are joined to each other via the layer $\mathcal{L}_\theta$ whose points are located near the line $\theta + \phi = 2\theta_{c0}$ and meet the inequality $\theta > \phi$ (see Fig. 5). So the left-hand side of the eigenvalue equation (23) is a monotonously increasing function of ζ and the solution of this equation ζ_c decreases as the potential θ increases for a fixed value of ϕ. The results obtained in the two previous subsections show us that the quantity ζ_c, first, drops from very large values up to $\zeta_c \gtrsim 1$ as the analyzed point $\{\theta, \phi\}$ goes from the instability boundary $\mathcal{B}_\theta$ to the layer $\mathcal{L}_\theta$. Then, just after the point crossing the layer $\mathcal{L}_\theta$, the quantity ζ_c takes values about $\zeta_c \lesssim 1$ and drops down to zero as the analyzed point goes away from it. In fact, on one hand, by virtue of Eq. (36) when the analyzed point $\{\theta, \phi\}$ tend to the layer $\mathcal{L}_\theta$ on the side of the domain $\mathcal{D}_\theta$ and inequality (42) holds we have

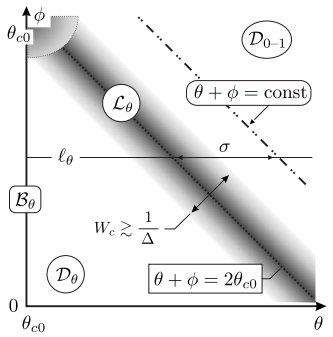

FIG. 5. The intermediate layer $\mathcal{L}_\theta$ separating the instability domains $\mathcal{D}_\theta$ and $\mathcal{D}_{0\text{-}1}$. Zoomed-in view.

$$\zeta_c = \frac{\sqrt{2}\Delta(2\theta_{c0} - \theta - \phi)}{\theta - \phi}.$$

On the other hand, for the point $\{\theta, \phi\}$ located near the layer $\mathcal{L}_\theta$ on the side of the domain $\mathcal{D}_{0\text{-}1}$ where the inequality (48) holds, the solution ζ_c of the eigenvalue equation (23) is approximated as

$$\zeta_c = \frac{\sqrt{2}\theta_{c0}}{\Delta(\theta + \phi - 2\theta_{c0})}$$

by virtue of Eq. (45). The "boundaries" of the layer $\mathcal{L}_\theta$ meet the estimate $\Delta|\theta + \phi - 2\theta_{c0}| \gtrsim 1$, which justifies the statement mentioned above. So inside the layer $\mathcal{L}_\theta$ the quantity ζ_c has to change in a region where $\zeta_c \sim 1$.

The expression obtained below for the critical value of the diffusion flux g_c is valid, however, for a wider region than the layer $\mathcal{L}_\theta$ itself due to the adopted assumption $\Delta \gg 1$. Namely, in this subsection we consider the region for which

$$|\theta + \phi - 2\theta_{c0}| \ll 1, \tag{51}$$

thereby the two inequalities

$$\zeta_c \Delta \gg 1 \quad \text{and} \quad \frac{\zeta_c}{\Delta} \ll 1 \tag{52}$$

hold simultaneously. This region comprises the layer $\mathcal{L}_\theta$ as well as the neighboring parts of the domains $\mathcal{D}_\theta$ and $\mathcal{D}_{0\text{-}1}$. So the expression for the diffusion flux threshold valid in it really specifies the crossover between the domains $\mathcal{D}_\theta$ and $\mathcal{D}_{0\text{-}1}$.

Under condition (52) the former term on the left-hand side of Eq. (23) can be approximated by the asymptotics of the function $\Psi_1(x)$ for $x \to \infty$, whereas the latter one matches

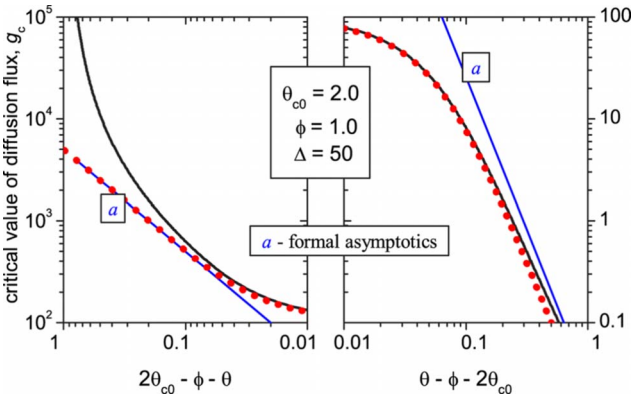

FIG. 6. (Color online) The critical value of the dimensionless diffusion flux g_c vs the nonideality parameter θ near the intermediate layer $\mathcal{L}_\theta$. The plot is based on the general equations (23) and (24) using the parameters shown in inset. The straight lines visualize the formal asymptotics (43) and (49) whereas the dotted line corresponds to Eq. (55).

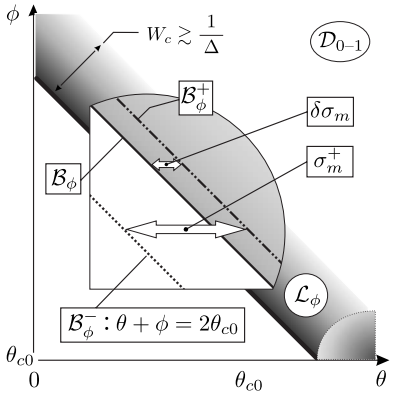

FIG. 7. The boundary layer $\mathcal{L}_\theta$ separating the instability domain $\mathcal{D}_{0\text{-}1}$ and the region of the stable crystal growth. Zoomed-in view with an additional magnifying lens showing the finite structure of the instability boundary $\mathcal{B}_\phi$.

the limit $x \to 0$. Therefore in this case Eq. (23) can be rewritten as

$$(\theta + \phi)\frac{1}{\zeta} - (\theta - \phi)\zeta = \sqrt{2}\Delta\sigma, \tag{53}$$

where σ is given by expression (50). The solution of Eq. (53) is of the form

$$\zeta_c = \frac{1}{\sqrt{2}(\theta - \phi)}[\sqrt{\Delta^2\sigma^2 + 2(\theta^2 - \phi^2)} - \Delta\sigma]. \tag{54}$$

Then the substitution of Eq. (54) into Eq. (24) yields

$$g_{c\{\mathcal{L}_\theta\}} = \frac{2\theta_{c0}\Delta\zeta_c^2}{\sqrt{\Delta^2\sigma^2 + 2(\theta^2 - \phi^2)}}, \tag{55}$$

where the function $\Psi_2(x)$ has been also approximated using the appropriate asymptotics. As it must be, expression (55) converts into expressions (43) and (49) for $\mp\Delta\sigma \gg 1$, respectively.

Figure 6 illustrates the obtained crossover of the diffusion flux threshold. In this figure the critical value g_c of the dimensionless diffusion flux is shown vs actually the nonideality parameter θ for fixed parameters ϕ=1 and Δ=50. In other words, it visualizes $g_c(\theta)$ for the analyzed point $\{\theta, \phi\}$ moving along the line ℓ_θ shown in Fig. 5.

D. Boundary layer $\mathcal{L}_\phi$

When the potential θ is less than the threshold θ_{c0} the solid nonideality cannot individually cause the system instability. In this case only the cumulative effect of the system nonideality and asymmetry gives rise to the growth instability or even the system asymmetry itself does when the potential ϕ is high enough. So for $\theta < \theta_{c0}$ the instability domain $\mathcal{D}_{0\text{-}1}$ borders with the region of the stable crystal growth via the boundary layer $\mathcal{L}_\phi$ (Fig. 7). Let us consider its properties in detail. As for the layer $\mathcal{L}_\theta$ analyzed in the previous subsection the given layer matches the root ζ_c of Eq. (23) of order unity, $\zeta_c \sim 1$. However, in this case by virtue of condition (28) the potential ϕ should exceed the nonideality parameter, $\phi > \theta$, for the growth instability to arise. As a result the two terms entering the left-hand side of Eq. (23) have opposite signs and the functions $\Psi_1(x)$, $\Psi_2(x)$ should be approximated to the next order in the corresponding small parameters in comparison with the case of the layer $\mathcal{L}_\theta$. Namely, using inequalities (52) expressions (23) and (24) are reduced to the equation

$$\frac{(\phi + \theta)}{\zeta} + (\phi - \theta)\zeta = \sqrt{2}\Delta\sigma + O\left(\frac{1}{\Delta^2}\right) \tag{56}$$

and the expression for the diffusion flux threshold

$$g_c = \frac{2\sqrt{2}\theta_{c0}\Delta\zeta^2}{\Phi(\zeta)}, \tag{57}$$

where the function $\Phi(\zeta)$ is introduced by the formula

$$\Phi(\zeta) := \left[\frac{(\phi + \theta)}{\zeta} - (\phi - \theta)\zeta\right] - \frac{\sqrt{2}}{\Delta}\left[\frac{(\phi + \theta)}{\zeta^2} - (\phi - \theta)\zeta^2\right] + O\left(\frac{1}{\Delta^2}\right). \tag{58}$$

It should be pointed out that expression (56) does not contain a term of order Δ^{-1} and the other term of order Δ^{-2} is not written explicitly because its effect is reduced only to a small constant contribution to the value of σ.

To explain the resulting dependence of the diffusion flux threshold g_c on the potential difference σ let us refer to Fig. 8. It illustrates the value of σ treated as a formal function of ζ that is determined by Eq. (56) and has a minimum σ_m meeting the estimate

$$\Delta\sigma_m = \sqrt{2(\phi^2 - \theta^2)} + O\left(\frac{1}{\Delta^2}\right) \tag{59}$$

and attained at

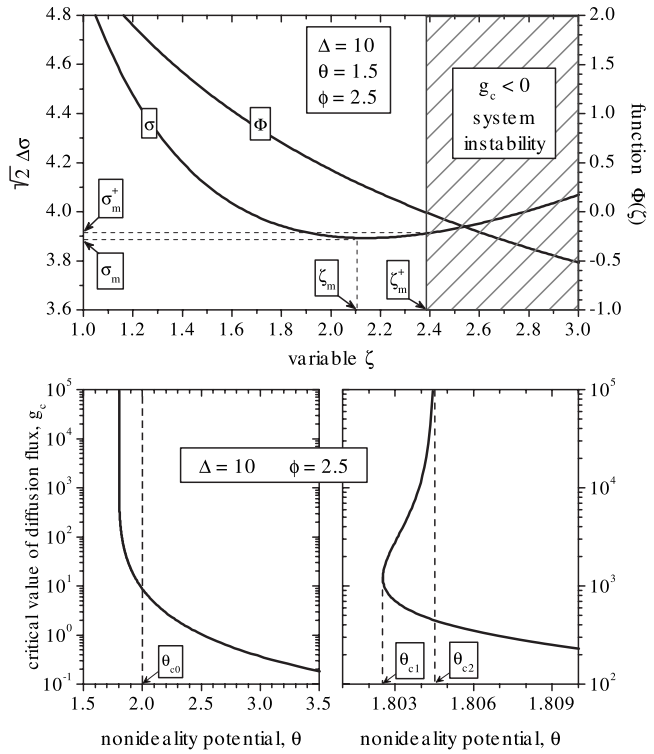

FIG. 8. Illustration of the mechanism responsible for the complex behavior of the critical diffusion flux in the boundary layer $\mathcal{L}_\phi$ (upper fragment) and the resulting $g_c(\theta)$ dependence (lower fragments). The right-hand fragment depicts this dependence in zoom, making it evident that in the region $(\theta_{c1}, \theta_{c2})$ the growth rate should belong to a bounded interval for the instability to arise. In plotting the potential difference σ as a formal function of the variable ζ determined by Eq. (56) and the function $\Phi(\zeta)$ [see Eq. (57)] vs the variable ζ the values $\theta=1.5$, $\phi=2.5$, and $\Delta=10$ were used as well as the original functions $\Psi_1(x)$ and $\Psi_2(x)$ [expression (25)] rather than their approximations were applied to take into account not only the leading terms but also all the other small contributions.

$$\zeta_m = \sqrt{\frac{\phi+\theta}{\phi-\theta}} + O\left(\frac{1}{\Delta^2}\right). \tag{60}$$

It matches the critical value of the species diffusion flux

$$g_m = \frac{\theta_{c0}\Delta^2}{\theta}\left(\frac{\phi+\theta}{\phi-\theta}\right) \tag{61}$$

written in the leading order of $1/\Delta$.

If the potential difference $\sigma=\phi+\theta-2\theta_{c0}$ is less than σ_m there is no solution of Eq. (56) [i.e., of Eq. (23)] and the crystal growth is stable. When $\sigma>\sigma_m$ Eq. (56) admits two solutions written again in the leading order of $1/\Delta$ as

$$\zeta_c^- = \sqrt{2}(\phi+\theta)[\Delta\sigma + \sqrt{\Delta^2\sigma^2 - 2(\phi^2-\theta^2)}]^{-1} \tag{62}$$

and

$$\zeta_c^+ = \frac{1}{\sqrt{2}(\phi-\theta)}[\Delta\sigma + \sqrt{\Delta^2\sigma^2 - 2(\phi^2-\theta^2)}]. \tag{63}$$

Solution (62) matches the decreasing branch of the dependence $\sigma(\zeta)$ (Fig. 8) and describes the lower boundary of the diffusion flux threshold $g_c(\sigma)$ obeying the estimate

$$\frac{g_m}{g_c(\sigma)} \approx \left(1+\frac{\Delta^2}{2\theta}\sqrt{\sigma^2-\sigma_m^2}\right)\left(\frac{\sigma+\sqrt{\sigma^2-\sigma_m^2}}{\sigma_m}\right)^2. \tag{64}$$

This branch actually specifies the minimal value $\theta_{c1}(\phi,\Delta)$ of the nonideality parameter θ necessary for the growth instability to arise for given values of the parameters ϕ and Δ, namely, by virtue of Eq. (59)

$$\theta_{c1} \approx 2\theta_{c0} - \phi + \frac{2\sqrt{2}}{\Delta}\sqrt{\phi-\theta_{c0}}. \tag{65}$$

As it must be, expression (64) converts into expression (49) for $\Delta\sigma \gg 1$ describing the behavior of the diffusion flux threshold in the instability domain $\mathcal{D}_{0\text{-}1}$ near the boundary layer $\mathcal{L}_\phi$.

Solution (63) describes the upper boundary of the instability region $g_c^+(\sigma)$ which, however, exists only within a rather narrow interval of the potential difference σ, i.e., when $\sigma_m<\sigma<\sigma_m^+$ (Fig. 8). The parameter σ_m^+ and the corresponding value ζ_m^+ match the point where the function $\Phi(\zeta)$ changes its sign passing through zero. Exactly at this point the upper branch $g_c^+(\sigma)$ of the diffusion flux threshold goes to infinity and for $\sigma>\sigma_m^+$, i.e., for $\zeta>\zeta_m^+$ it does not exist. In this case the values of the species diffusion flux corresponding to the instability onset are bounded only from below by the threshold $g_c(\sigma)$. According to expressions (56) and (57) the difference between ζ_m and ζ_m^+ is a value of the first order in the parameter $1/\Delta$, namely,

$$\zeta_m^+ - \zeta_m = \frac{\sqrt{2}\theta}{\Delta(\phi-\theta)}, \tag{66}$$

and as a result the corresponding difference of the parameters is

$$\delta\sigma_m := \sigma_m^+ - \sigma_m = \frac{\sqrt{2}\theta^2}{\Delta^3\sqrt{\phi^2-\theta^2}}. \tag{67}$$

The obtained expression demonstrates the fact that this difference specifying the thickness of the region where the diffusion flux threshold exhibits complex behavior is extremely narrow (Fig. 8). It is of the third order in the small parameter $1/\Delta$ and can be ignored. In this case only the first term in expansion (58) should be taken into account thus only branch (59) exists. So by virtue of Eq. (64) the diffusion flux threshold in the layer $\mathcal{L}_\phi$ as well as in its small neighborhood meeting the interval $\sigma_m<\sigma\ll 1$ is approximated by the expression

$$g_c(\sigma) \approx \frac{16\theta_{c0}^3}{\sqrt{\sigma^2-\sigma_m^2}(\sigma+\sqrt{\sigma^2-\sigma_m^2})^2} \tag{68}$$

showing some formal singularity when $\sigma\to\sigma_m+0$.

Finalizing this subsection let us discuss the behavior of the instability boundary $\mathcal{B}_\phi$ depending on the parameter Δ including its relatively small values. It should be reminded that previously we considered two curves on the plane $\{\theta,\phi\}$, the instability boundary $\mathcal{B}_\phi=\{\phi_c(\theta)\}$ itself and the curve $\mathcal{B}_\phi^+=\{\phi_c^+(\theta)\}$. The former singles out the points on this plane

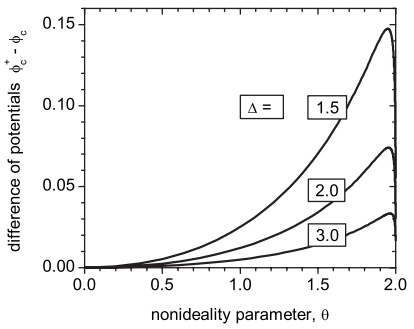

FIG. 9. The difference in the instability boundaries $\mathcal{B}_\phi^+$ and $\mathcal{B}_\phi$ for several values of the parameter Δ.

where the crystal growth can become unstable for some values of the species diffusion flux. The latter is the boundary of the growth instability for vary large values of the diffusion flux, $g \to \infty$.

It can be demonstrated analyzing directly the general eigenvalue equation (23) and the expression (24) for the critical diffusion flux g_c that the terminal points of the curves $\mathcal{B}_\phi$ and $\mathcal{B}_\phi^+$ at $\theta=0$ and $\theta=\theta_{c0}$ coincide with each other for a given value of Δ. So by virtue of expression (33) their coordinates are specified by the following expressions:

$$\phi_0 = 2\theta_{c0}\frac{\Delta^2+\sqrt{2}\Delta+1}{\Delta^2-1} \quad \text{for } \theta=0, \tag{69}$$

$$\phi_{c0} = \theta_{c0}\frac{\Delta^2+1}{\Delta^2-1} \quad \text{for } \theta=\theta_{c0}. \tag{70}$$

As it must, the ϕ coordinates of both the points have a singularity as $\Delta \to 1$ because in this limit the growth is stable for $\theta < \theta_{c0}$.

For the intermediate points $0<\theta<\theta_{c0}$ the curves $\mathcal{B}_\phi$, $\mathcal{B}_\phi^+$ deviate from each other. To evaluate this difference Fig. 9 plots the difference $\phi_c^+ - \phi_c$ vs the potential θ for several values of Δ. As seen in Fig. 9 the curves $\mathcal{B}_\phi$ and $\mathcal{B}_\phi^+$ practically coincide with each other except for the values of Δ coming too close to its threshold $\Delta=1$. Thereby expression (33) gives a fairly fine approximation of the instability boundary $\mathcal{B}_\phi$ for such values of Δ.

E. Double critical point and its neighborhood $\mathcal{C}$

The boundaries $\mathcal{B}_\theta$ and $\mathcal{B}_\phi$ of the instability region meet at the point $\{\theta_{c0}, \phi_{c0}\}$ that can be referred to as a double critical point because its coordinates are the threshold of the nonideality parameter and the threshold of the asymmetry potential exceeding which the system asymmetry changes the instability property substantially (see Fig. 10). The latter implies the fact that the asymmetry causes the instability onset in the system being stable before the potential exceeds the threshold, $\phi > \phi_{c0}$, and ϕ_{c0} is the minimal value possessing this property among all the possible values of the solid composition χ and the nonideality parameter θ. Therefore in calculating the value of ϕ_{c0} we can set $\theta=\theta_{c0}$.

The critical region $\mathcal{C}$ is a certain neighborhood of the point $\{\theta_{c0}, \phi_{c0}\}$ where the layers $\mathcal{L}_\theta$ and $\mathcal{L}_\phi$ overlap with

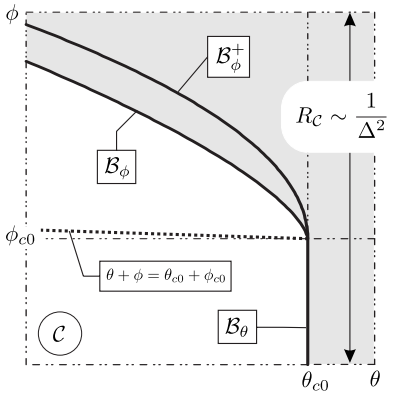

FIG. 10. Structure of the instability region in a close proximity to the double critical point $\{\theta_{c0}, \phi_{c0}\}$.

each other. So it should exhibit some crossover between the properties of these layers. According to the results to be obtained in the region $\mathcal{C}$ the potential difference $\phi-\theta$ is rather small so not only the inequality $\zeta_c\Delta \gg 1$ but also $\zeta_c/\Delta \gg 1$. Keeping in mind the general condition (28) which is necessary for the system asymmetry to affect essentially the instability onset, we describe the region $\mathcal{C}$ with two small parameters $u \ll 1$ and $v \ll 1$ introduced as follows:

$$(\phi-\theta) = \frac{\phi+\theta}{\Delta^2}(1+u),$$

$$(\theta-\theta_{c0}) = \frac{\phi+\theta}{2\sqrt{2}\Delta^2}v. \tag{71}$$

Then for the variable $\xi := \Delta/\zeta \ll 1$ regarded as a small value the eigenvalue equation (23) is reduced to

$$v = -xu + x^3 \tag{72}$$

and expression (24) for the diffusion flux threshold takes the form

$$g_{c\{\mathcal{C}\}} = \frac{4\sqrt{2}\Delta^4}{(\theta+\phi)}\frac{1}{x^2(x\sqrt{2}-u)}. \tag{73}$$

As it must, when $u<0$ the instability boundary is specified by the equality $v=0$ $(\theta=\theta_{c0})$ and the diffusion flux threshold $g_c \to \infty$ as $v \to +0$. For $u>0$ the system changes the behavior.

The eigenvalue equation (72) relating the variables u and v at the point $x=\sqrt{u/3}$ where its right-hand side attains the minimum specifies the instability boundary $\mathcal{B}_\phi$, namely,

$$v = -\frac{2}{3\sqrt{3}}u^{3/2} \tag{74a}$$

or returning to the variables θ and ϕ

$$\frac{\theta-\theta_{c0}}{\theta_{c0}} = -\frac{\Delta}{6\sqrt{3}}\left(\frac{\phi-\phi_{c0}}{\phi_{c0}}\right)^{3/2}. \tag{74b}$$

As should be expected, at the boundary $\mathcal{B}_\phi$ the diffusion flux threshold takes a finite value equal to

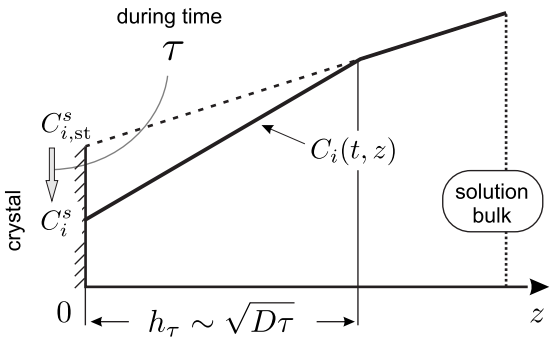

FIG. 11. Perturbation of the species distribution in the aqueous solution induced by variations in the surface concentration C_i^s on time scales about τ. Schematic illustration.

$$g_{c\{\mathcal{C}|\mathcal{B}_\phi\}} = 6\sqrt{6}\Delta\left(\frac{\phi_{c0}}{\phi-\phi_{c0}}\right)^{3/2}. \tag{75}$$

Naturally, the diffusion flux threshold g_c diverges as the asymmetry potential $\phi \to \phi_{c0}+0$.

Near the boundary $\mathcal{B}_\phi$ the values of the diffusion flux causing the instability onset are bounded from below and above. The locus $\mathcal{B}_\phi^+$ where the upper boundary goes to infinity is specified by the singularity point of function (73), i.e., $x=u/\sqrt{2}$. This value via equality (72) gives us the relationship between the potentials θ and ϕ at the curve $\mathcal{B}_\phi^+$,

$$v = -\frac{1}{\sqrt{2}}u^2 \tag{76a}$$

or

$$\frac{\theta-\theta_{c0}}{\theta_{c0}} = -\frac{\Delta^2}{16}\left(\frac{\phi-\phi_{c0}}{\phi_{c0}}\right)^2. \tag{76b}$$

The expressions obtained here hold for $u,v \ll 1$, so the characteristic size of the region of double criticality is about $R_c \sim 1/\Delta^2$.

V. REGIMES OF INSTABILITY DYNAMICS

The present section is devoted to a qualitative analysis of the system dynamics. For the sake of simplicity we ignore difference in the species kinetic coefficients setting $D_1=D_2=D$ and $\nu_1=\nu_2$.

At first, let us consider perturbations of the species distribution $\delta C_i(z,t)$ induced by small variations $\delta\chi(t)$ in the surface composition on time scales about τ. Actually $1/\tau$ is the perturbation increment analyzed in the previous section. Change in the surface composition $\chi(t)$ affects directly the species attachment rate caused by the growth process, which, in turn, gives rise to variations in the species concentration near the crystal surface δC_i^s. These boundary variations in the species concentration spread into the solution bulk, which is responsible for the formation of spatial perturbations in the species distribution schematically shown in Fig. 11. The characteristic spatial scale of these perturbations can be estimated as $h_\tau \sim (D\tau)^{1/2}$.

Within a qualitative approximation mass conservation for such perturbations reads

$$-\frac{h_\tau \delta C_i^s}{\tau} \sim \delta[r_i(C_i^s,\chi)] \tag{77}$$

or, by virtue of Eq. (12),

$$-\frac{h_\tau}{\tau}\delta C_i^s \sim \frac{a}{\tau_i}\delta C_i^s + \frac{aC_{i,\mathrm{st}}}{\tau_i}\omega_i\delta\chi, \tag{78}$$

where the quantities (for $i=1,2$)

$$\omega_i(\chi_{\mathrm{st}}) = -\left.\frac{d\ln\tau_i(\chi)}{d\chi}\right|_{\chi=\chi_{\mathrm{st}}} \tag{79}$$

have been introduced and by virtue of Eq. (13)

$$\omega_1 = \phi+\theta, \quad \omega_2 = \phi-\theta. \tag{80}$$

Expression (78) enables us to single out two limit cases. The first one which will be referred to as *the growth regime of constant growth rate* matches rather slow variations of the crystal composition χ, and the species concentration C_i, namely, the condition $\tau \gg \tau_i(h_\tau/a)$ or, what is the same,

$$\tau \gg \frac{D\tau_i^2}{a^2}. \tag{81}$$

In this case Eq. (78) yields

$$\delta C_i^s \approx -C_{i,\mathrm{st}}^s\omega_i\delta\chi \tag{82}$$

and thus, via Eq. (77),

$$\delta[r_i(C_i^s,\chi)] \sim \left(\frac{D\tau_i^2}{\tau a^2}\right)^{1/2} r_{i,\mathrm{st}} \ll r_{i,\mathrm{st}}. \tag{83}$$

We note that the factor $\omega_i\delta\chi$ has been omitted in estimate (83) because the typical values of ω_i under consideration are of order unity as well as variations of the solid composition χ during the growth dynamics are about unity. Thereby for slow variations of the crystal composition χ the induced perturbations in the species distribution $C_i(z,t)$ are in quasiequilibrium. In other words, the boundary value C_i^s of the species concentration changes in time with χ in such a manner that the boundary value of the diffusion flux, the species attachment rate r_i, be practically equal to the inflow of the corresponding species at distant points. In particular, exactly such variations are described by expression (82) being linearization of the condition

$$\frac{aC_i^s}{\tau_i(\chi)} = r_i \approx \mathrm{const}. \tag{84}$$

The second limit case, which will be called *the growth regime of constant surface concentration* is related to rather fast variations in the crystal composition χ, when their time scale τ meets the inequality $\tau \ll \tau_i(h_\tau/a)$ or

$$\tau \ll \frac{D\tau_i^2}{a^2}. \tag{85}$$

In this case the induced variations in the surface concentration C_i^s of species i are rather small in comparison with that could be expected in the previous limit case,

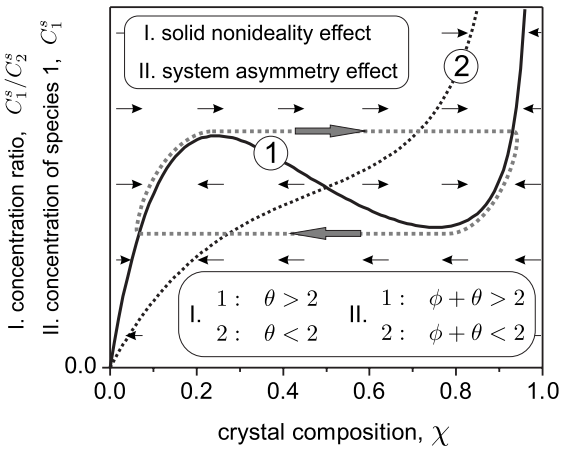

FIG. 12. Phase planes demonstrating the mechanism of the instability onset caused by the solid nonideality (I) and the system asymmetry (II).

$$\delta C_i^s \sim -\left(\frac{\tau a^2}{D\tau_i^2}\right)^{1/2} \omega_i C_{i,\mathrm{st}}^s \delta\chi \ll \omega_i C_{i,\mathrm{st}}^s \delta\chi. \tag{86}$$

Therefore at the first approximation the fast dynamics of the species distribution and the crystal composition meets the equalities

$$C_i^s \approx \text{const} \quad \text{and} \quad \delta r_i \approx a C_i^s \delta\left(\frac{1}{\tau_i(\chi)}\right). \tag{87}$$

In this consideration the variations of the crystal composition $\chi(t)$ were treated to be given beforehand. In order to draw some conclusions about the growth dynamics as a behavior of an autonomous system it is necessary to discuss how the induced variations of the attachment rates r_1 and r_2 affect, in their turn, the crystal composition χ. This effect is described by the governing equation (15).

As was discussed in the previous section, when the nonideality potential exceeds the critical value, $\theta > \theta_{c0}$ the perturbation increment $1/\tau \to \infty$ as the species diffusion flux goes to infinity also. So it is natural to expect that for the developed instability the regime of constant surface concentration takes place with respect to *both* the species components. Then keeping in mind expressions (87) and applying to Eq. (15) governing the dynamics of crystal composition we can draw the velocity field of the system motion on the phase plane $\{C_1^s/C_2^s, \chi\}$ as shown in Fig. 12. The curve

$$\frac{C_1^s}{C_2^s} = \frac{\chi}{(1-\chi)}\frac{\tau_1(\chi)}{\tau_2(\chi)} \propto \frac{\chi}{(1-\chi)} e^{-2\theta\chi} \tag{88}$$

divides this phase plane into parts with the opposite directions of the velocity field. In obtaining Eq. (88) expressions (13) have been used. As it should be the stationary values of the species concentrations $C_{i,\mathrm{st}}^s$ and the crystal composition χ_{st} [see expressions (84)] meet equality (88). Figure 12 clearly demonstrates that under such conditions its increasing branches are stable whereas a decreasing branch (if it exists) is unstable. So the limit circle at a rough approximation should have the form shown in Fig. 12. Exactly this limit was analyzed in our previous paper [11] and corresponds to the domain $\mathcal{D}_\theta$ of the instability region.

If the nonideality parameter θ is less than the critical value, $\theta < \theta_{c0}=2$ the solid nonideality cannot itself induce the growth instability. In this case the instability development is governed by the system asymmetry, which is reflected in properties of the instability domain $\mathcal{D}_{0\text{-}1}$. In particular, for the system with such parameters only the channel 0-1 of the precipitation reactions (1) plays an active role, the channel 0-2 is characterized by the equilibrium value of the species diffusion flux at the crystal surface. In this case it is quite natural to assume that the perturbation increment $1/\tau$ meets the inequality

$$\frac{D\tau_2}{a^2} \ll \tau \ll \frac{D\tau_1}{a^2}. \tag{89}$$

Therefore, on one hand, with respect to species 2 such a process can be classified within the regime of constant growth rate. On the other hand, with respect to species 1 the regime of constant surface concentration takes place. Actually it is the case for the points of the domain $\mathcal{D}_{0\text{-}1}$. To describe the corresponding dynamics of the crystal composition χ we can fix the surface concentration C_1^s and set the species attachment rate $r_2=(1-\chi_{\mathrm{st}})G$. Then we draw a similar velocity field of the system motion on the phase space $\{C_1^s, \chi\}$ shown again in the same Fig. 12. Its pattern is identical to one discussed above except for the fact that the y axis of this phase plane has now another meaning, it presents the surface concentration of species 1. As follows from Eq. (15) and expressions (13) the curve

$$C_1^s = \frac{\chi}{(1-\chi)}\tau_1(\chi)\frac{\chi_{\mathrm{st}}G}{a} \propto \frac{\chi}{(1-\chi)} e^{-(\theta+\phi)\chi} \tag{90}$$

separates the regions on the phase plane $\{C_1^s, \chi\}$ with the opposite directions of the velocity field. This curve looks like the previous one, Eq. (88), within the replacement $2\theta \to \theta + \phi$. So again the instability condition for the potentials of the species interactions take the form $\theta + \phi > 2\theta_{c0}$, being in agreement with the results obtained before. As previously the increasing branches of curve (90) are stable whereas the decreasing one is unstable and the system transition between them as well as the transition from the unstable stationary point $\{C_{1,\mathrm{st}}^s, \chi_{\mathrm{st}}\}$ to one of them proceeds within the regime of constant surface concentration with respect to species 1. The rough approximation of the limit circle again has the same form.

In the part of the domain $\mathcal{D}_{0\text{-}1}$ where $\theta > \theta_{c0}$ both of the instability scenarios can be implemented. So depending on the species diffusion flux either the phase plane $\{C_1^s, \chi\}$ or the plane $\{C_1^s/C_2^s, \chi\}$ can give an appropriate representation of the system dynamics.

VI. NONLINEAR DYNAMICS OF SYSTEM INSTABILITY: DOMAIN $\mathcal{D}_\phi$

This section presents numerical results for the system dynamics when the growth instability arise in a subdomain $\mathcal{D}_\phi$ of the domain $\mathcal{D}_{0\text{-}1}$, where the nonideality parameter θ is less

than its threshold, i.e., $\theta < \theta_{c0}$. So it is the system asymmetry that causes the instability.

To model numerically the system dynamics the governing equations (9)–(11) and (15) were converted into dimensionless form. Namely, first, the time t and the spatial coordinate z are measured in units,

$$\tau^* = \frac{\sqrt{D_1 D_2}\tau_g^2}{a^2}, \quad z^* = \frac{\sqrt{D_1 D_2}\tau_g}{a}, \tag{91}$$

respectively, i.e., the dimensionless time and spatial coordinates are introduced as $t_{\text{new}} = t_{\text{old}}/\tau^*$ and $z_{\text{new}} = z_{\text{old}}/z^*$. Second, the species concentrations and the diffusion flux are replaces with their dimensionless analogies, $C_{i,\text{new}} = C_{i,\text{old}}/C^*$ and $G_{i,\text{new}} = G_{i,\text{old}}/G^*$, where

$$C^* = \frac{1}{\sqrt{D_1 D_2}\tau_g a}, \quad G^* = \frac{1}{\sqrt{D_1 D_2}\tau_g^2}. \tag{92}$$

In this way the original model is rewritten in the form

$$\frac{\partial C_i}{\partial t} = \kappa_i \frac{\partial^2 C_i}{\partial z^2}, \tag{93}$$

$$\frac{d\chi}{dt} = [(1-\chi)\varrho_1(\chi)C_1^s - \chi\varrho_2(\chi)C_2^s], \tag{94}$$

with Eq. (93) being subject to the boundary condition at $z = 0$,

$$\kappa_i \left.\frac{\partial C_i}{\partial z}\right|_{z=0} = \varrho_i(\chi)C_i^s, \tag{95}$$

and the condition at distant points, i.e., at the formal external boundary $L_{\text{new}} = L_{\text{old}}/z^*$,

$$G_i = \kappa_i \left.\frac{\partial C_i}{\partial z}\right|_{z=L}. \tag{96}$$

Here the dimensionless species diffusivities are

$$\kappa_1 = \frac{1}{\kappa_2} = \sqrt{\frac{D_1}{D_2}} \tag{97}$$

and the dimensionless rates of the atom attachment to the growing crystal are

$$\varrho_1(\chi) = \varkappa_1 \exp\{\phi\chi - \theta(1-\chi)\},$$

$$\varrho_2(\chi) = \varkappa_2 \exp\{-\phi(1-\chi) - \theta\chi)\} \tag{98}$$

with

$$\varkappa_1 = \frac{1}{\varkappa_2} = \left(\frac{\nu_1}{\nu_2}\right)^{1/2} \exp\left\{-\frac{1}{2}\eta\right\}. \tag{99}$$

It should be noted that the previously used parameter Δ_ϕ is related to the introduced kinetic coefficients as

$$\frac{\varkappa_2}{\varkappa_1} = \left(\frac{\kappa_2}{\kappa_1}\right)^{1/2} e^{\phi}\Delta_\phi^2. \tag{100}$$

So the ratio $(\varkappa_1/\varkappa_2)e^{\phi}$ is actually the main small parameter of the given model because for aqueous solutions the relationship $D_1 \sim D_2$ is typically fulfilled.

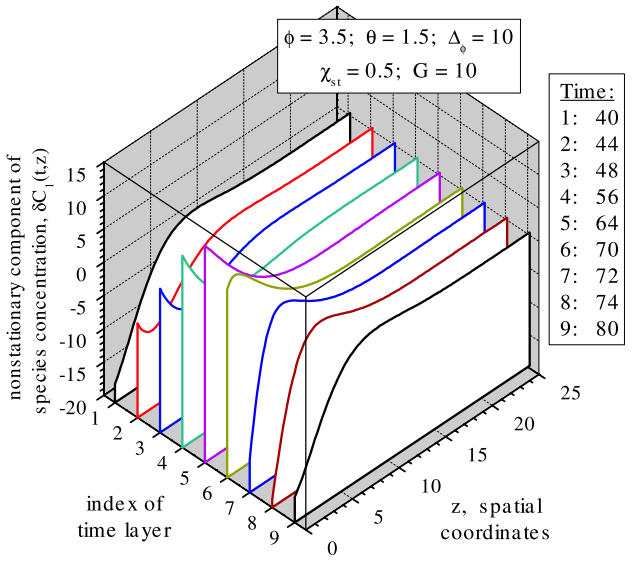

FIG. 13. (Color online) The time dependent component $\delta C_1(t,z)$ of the species 1 distribution in the aqueous solution bulk near the crystal surface, $z=0$, for several time slices within one period of the oscillations. Result of numerical simulation. The shown time origin $t=0$ is placed at an arbitrary chosen point that corresponds to the instability becoming well developed.

The system of equations (93)–(96) was solved numerically using the Crank-Nicholson scheme for the diffusion equation (93) and the midpoint method for Eq. (94). To exemplify the basic characteristics of the instability dynamics in the region $\mathcal{D}_\phi$ the system parameter were set equal to $\theta = 1.5$, $\phi = 3.5$, and $\Delta_\phi = 10$ as well as $\kappa_1 = \kappa_2 = 1$. Then expression (100) gave us the values of $\varkappa_1$ and $\varkappa_2$. The time and spatial steps in the simulation routine were 0.01; decreasing the steps twice did not affect the obtained results. The time variations in the species distribution induced by the developed instability turned out to be located near the crystal boundary within a layer of thickness about 15–20 spatial units. So the external boundary of the system was placed at $L = 100$, where the species concentrations C_1^∞ and C_2^∞ were fixed in such a way that the total diffusion flux and the solid composition take the values $G^{\text{st}} = G_1^{\text{st}} + G_2^{\text{st}} = 10$ and $\chi^{\text{st}} = 0.5$ under the steady state conditions. The total simulation time was 10 000 time units.

Below we will present the obtained results. Figure 13 visualizes evolution of the species distribution in the aqueous solution bulk near the crystal surface. Only the distribution of species 1 is shown because it, first, exemplifies similar effects for species 2 also and, second, plays the leading role in the instability onset. To elucidate the dynamics of the species distribution the time dependent component $\delta C_1(t,z)$ is singled out from the total distribution function,

$$C_1(t,z) = \delta C_1(t,z) + \langle C_1^s \rangle + \frac{\langle G_1 \rangle}{\kappa_1} z,$$

and depicted in Fig. 13. The other terms in this expression are the steady state components of the species distribution. As seen in this figure the time variations of species distribution are located near the crystal surface $z=0$ in its neighbor-

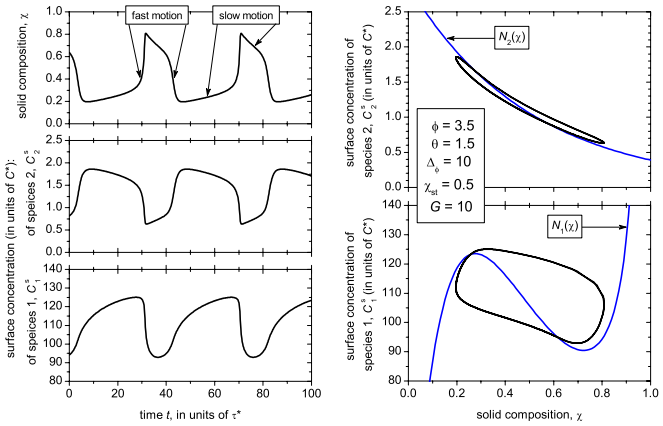

FIG. 14. (Color online) The dynamics of solid composition $\chi(t)$ and the surface species concentrations $C_i^s(t)$ (left column) and the corresponding phase portraits on the planes $\{\chi, C_i^s\}$ (right column). Result of numerical simulation. The shown time origin $t=0$ is placed at an arbitrary chosen point that corresponds to the instability becoming well developed and steady state.

hood of thickness about $L_C \sim 15$ for the chosen system parameters. So the size of the system $L=100$ used in the numerical simulations is fairly large to enable one to regard the external boundary $z=L$ as infinitely distant points. In any case in numerical simulations the size of the system should be specified that the inequality $L_C \lesssim L$ to hold.

Figure 13 demonstrates the fact that a simple model of the boundary layer similar to the one shown in Fig. 11 can be used only for a qualitative analysis. The actual spatial form of $\delta C_1(t,z)$ can possess a remarkable extremum attained at a certain internal point of the crystal neighborhood, which must be taken into account in constructing an appropriate boundary layer approximation.

Nevertheless, in spite of a rather rough model for the boundary layer used in Sec. V the instability scenarios described there is justified by the results of numerical simulation. The found dynamics of the solid composition $\chi(t)$ and the surface species concentrations $C_i^s(t)$ exhibit relaxation oscillations with clearly visible fast and slow stages of system motion (Fig. 14). So the results obtained for the given set of parameters do describe an essentially nonlinear regime of the growth instability. The phase portrait of the system oscillations on the plane $\{\chi, C_2^s\}$ demonstrates the fact that the regime of constant growth rate really takes place with respect to the species 2. Indeed the image of the oscillation limit circle on this phase plane is located in the vicinity of the curve $N_2(\chi)$ obtained by setting the right-hand side of the boundary condition (95) equal to the diffusion flux of species 2 under the stationary conditions, i.e.,

$$\varrho_2(\chi) C_2^s = (1-\chi_{\mathrm{st}}) G$$

and thus

$$N_2(\chi) = \frac{(1-\chi_{\mathrm{st}}) G e^{\phi}}{\varkappa_2} \exp\{-(\phi-\theta)\chi\}. \tag{101}$$

With respect to species 1 the regime of constant surface concentration could be expected to be the case. The image of the oscillation limit circle on the plane $\{\chi, C_1^s\}$ (Fig. 14) justifies this expectation at least within semiquantitative consideration. Figure 14 depicts the obtained limit circle together with the nullcline $N_1(\chi)$ constructed by setting the right-hand side of the governing equation (94) equal to zero, fixing the surface concentration C_1^s and assuming the attachment rate $\varrho_2(\chi) C_2^s$ of species 2 to meet the regime of constant diffusion flux. In this the expression

$$N_1(\chi) = \frac{(1-\chi_{\mathrm{st}}) G e^{\theta}}{\varkappa_1} \frac{\chi \exp\{-(\phi+\theta)\chi\}}{(1-\chi)} \tag{102}$$

has been constructed. As seen, here the fragments of the limit circle matching the fast motion deviate substantially from the decreasing branch of the nullcline $N_1(\chi)$ and the fragments of slow motion go near its increasing branches. So, roughly speaking, it is the characteristics of the nullcline $N_1(\chi)$ that specify the amplitudes of time variations in the solid composition and surface species concentrations for the developed growth instability. However, the obtained limit circle also deviates remarkably from a simple form constructed in Fig. 12 applying directly to the notions of the standard relaxation oscillations. The matter is that the system under consideration is really not reduced to a two-variable model implying actually the too simple boundary layer approximation shown in Fig. 11 to hold. So the dynamics of the surface concentration $C_1^s(t)$ of species 1 contains the fragments of slow motion as well as that of fast motion (Fig. 14). The latter ones actually force the fast motion branches of the limit circle to deviate remarkably from horizontal lines on the plane $\{\chi, C_1^s\}$. This effect was also observed for the growth instability caused by the solid nonideality [11].

Finalizing the present section we underline once more that there is a widely used approach to constructing the limit circle of oscillations in such a system, i.e., the "boundary reaction—diffusion" systems treating the governing equation (94) [or its original version (15)] for the solid composition in a too simple way. It sets the right-hand side of this equation equal to zero and relates the system portrait on the plane $\{\chi, (C_1^s/C_2^s)\}$ to the nullcline $N_{12}(\chi)$ determined by the expression

$$N_{12}(\chi) = \frac{\chi}{(1-\chi)} \frac{\varrho_2(\chi)}{\varrho_1(\chi)} = \frac{\varkappa_2 e^{-\phi}}{\varkappa_1} \frac{\chi \exp\{\theta(1-2\chi)\}}{(1-\chi)}. \tag{103}$$

For the growth instability caused by the solid nonideality the nullcline $N_{12}(\chi)$ possesses a decreasing unstable branch (see, e.g., Fig. 12). In this case the limit cycle constructed following the classical ideas of the standard relaxation oscillations is justified at least within a quasiqualitative analysis [11]. However, if the growth instability is induced by the system asymmetry, such an approach is not justified at all, the corresponding nullcline $N_{12}(\chi)$ is a monotonous curve and the system portrait on the plane $\{\chi, (C_1^s/C_2^s)\}$ is just located in its vicinity (Fig. 15).

VII. CONCLUSION

We have analyzed oscillatory zoning, i.e., the self-organization phenomenon arising during crystallization of

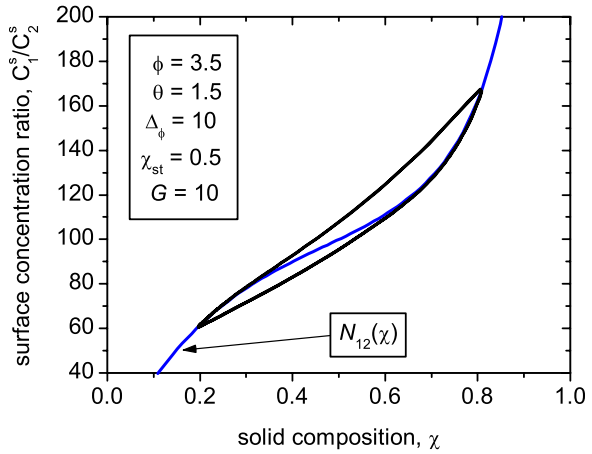

FIG. 15. (Color online) The phase portrait of the system oscillations on the plane $\{\chi,(C_1^s/C_2^s)\}$. Results of numerical simulation.

multicomponent solid from aqueous solution. It manifests itself in self-formation of quasiperiodic spatial patterns of solid composition from the core of a crystallite to its rim.

Keeping in mind systems like $(Ba,Sr)SO_4$, we have proposed a model for the growth of ternary-component solid from aqueous solution. The crystallization process comprises passive diffusion of species towards the crystal surface through the aqueous solution bulk, their adsorption at the crystal surface, and incorporation into the crystalline lattice at the surface atomic steps. The latter process is assumed to limit the crystal growth, so the species adsorption-desorption at the crystal surface is described within the quasiequilibrium approximation. Due to a very low rate of crystallization from aqueous solutions the growth dynamics is simulated using the boundary-reaction-diffusion model for the species distribution in the aqueous solution bulk.

The proposed model for the growth process takes into account the solid nonideality as well as the system asymmetry, with the latter being the characteristic feature of systems for which oscillatory zoning was reproduced under controlled conditions. It has been demonstrated that the system asymmetry can cause the growth instability in the case when the solid nonideality is low, i.e., the nonideality parameter is less than its threshold, $\theta<\theta_{c0}$, or even if the solid solution is ideal, $\theta=0$. Using the linear stability analysis the instability domain is constructed in the phase space $\{\theta,\phi,\Delta,g\}$ comprising the nonideality parameter θ, the difference ϕ of the species interaction constants, the parameter Δ characterizing the ratio between time scales of species incorporation into the crystalline lattice, and the species diffusion flux (in dimensionless units). The potential difference $\phi>0$ is assumed beforehand to be non-negative because, otherwise, exchanging the species indices makes it value positive. Projection of this domain onto the plane $\{\theta,\phi\}$ for a fixed value of Δ enables us to divide all the points on the plane $\{\theta,\phi\}$ into stable and unstable ones. The latter points correspond to such solids for which the growth instability under consideration can arise in principle.

It has been demonstrated that there are five characteristic regions on the plane $\{\theta,\phi\}$, where the growth instability exhibits different properties. In particular, in the region

$$\{\theta>\theta_c;\theta+\phi<2\theta_{c0}\}$$

the growth instability is governed mainly by the solid nonideality and was analyzed in detail previously in Ref. [11]. In the region

$$\{\theta>\theta_c;\theta+\phi>2\theta_{c0}\}$$

for $\Delta\gg1$ the instability onset is governed by the system asymmetry and, as a result, only one species plays an active role, the diffusion flux of the other component is practically quasiequilibrium. However, for large values of the diffusion flux the instability dynamics again is mainly affected by the solid nonideality. In the region

$$\{\theta<\theta_c;\theta+\phi>2\theta_{c0}\}$$

for $\Delta\gg1$ the instability is due to the system asymmetry even for large values of the diffusion flux. It can arise also for the ideal solid solution.

In this case the critical value g_c of the species diffusion flux exhibits a rather complex behavior near the instability boundary. In particular, g_c remains bounded as the system comes close to it. It has been demonstrated that the system asymmetry can induce, in principle, the growth instability if $\Delta>1$. However, if $\Delta\to1$ the required value of the potential difference ϕ_c approaches to ∞ (for a fixed value of $\theta<\theta_{c0}$). The condition that the system admits an unstable perturbation with finite spatial scales for large values of the species diffusion flux, $g\to\infty$, gives a fairly precise approximation of the boundary of the instability caused by the system asymmetry except for values of Δ close to its threshold $\Delta=1$.

Analyzing the limit cases of the growth dynamics two typical regimes were singled out. One of them is the regime of constant diffusion flux that characterizes "slow" dynamics of species concentration and solid composition. The other referred to as the regime of constant surface concentration described the stage of "fast" dynamics. Oscillatory zoning studied in our previous paper [11] corresponds to the case when the region of constant surface concentration holds with respect to all the species. As a result the phase portrait of the system dynamics looks like a limit circle of relaxation oscillations in the phase plane $\{C_1^s/C_2^s,\chi\}$. At a rough approximation it can be constructed referring to the N-like curve showing the quasistationary dependence of the ratio C_1^s/C_2^s on χ. In the present paper the main attention is paid to the case $\Delta\gg1$ where the nonlinear stage of the developed instability is characterized by the regime of constant surface concentration with respect to one species and regime of constant diffusion flux with respect to the other species. Now the phase plane $\{C_1^s,\chi\}$ gives the appropriate representation of the system portrait in a similar way, including the construction of the limit circle describing oscillatory zoning.

Numerical simulation justifies these conclusions. Besides, the species distribution in the aqueous solution bulk found

numerically demonstrates the fact that a rather sophisticated model of the boundary layer should be developed to describe oscillatory zoning adequately.

In the next step the spatial aspects of the surface properties will be taken into account by extending the present analysis by a surface dimension. Then the possible emergence of new characteristic length scales along the surface can be checked.

ACKNOWLEDGMENTS

One of the authors (I.L.) appreciates the financial support of the SFB 458 and the University of Munster as well as the partial support of DFG Grant No. MA 1508/8-1 and RFBR Grant No. 06-08-89501. The authors also thank A. Putnis for helpful discussions.

[1] M. Shore and A. D. Fowler, Can. Mineral. **34**, 1111 (1996).
[2] R. J. Reeder, R. O. Fagioli, and W. J. Meyers, Earth-Sci. Rev. **29**, 39 (1990).
[3] A. Putnis, L. Fernandez-Diaz, and M. Prieto, Nature (London) **358**, 743 (1992).
[4] C. M. Pina, M. Enders, and A. Putnis, Chem. Geol. **168**, 195 (2000).
[5] M. Prieto, A. Putnis, and L. Fernandez-Diaz, Geol. Mag. **130**, 289 (1993).
[6] P. J. Ortoleva, *Geochemical Self-Organization* (Oxford University Press, New York, 1994).
[7] P. J. Ortoleva, Earth-Sci. Rev. **29**, 3 (1990).
[8] I. L'Heureux and B. Jamtveit, Geochim. Cosmochim. Acta **66**, 417 (2002).
[9] S. Katsev and I. L'Heureux, Phys. Rev. E **66**, 066206 (2002).
[10] I. L'Heureux and S. Katsev, Chem. Geol. **225**, 230 (2006).
[11] F. Kalischewski, I. Lubashevsky, and A. Heuer, Phys. Rev. E **75**, 021601 (2007).
[12] M. Prieto, A. Fernandez-Gonzalez, A. Putnis, and L. Fernandez-Diaz, Geochim. Cosmochim. Acta **61**, 3383 (1997).
[13] P. D. Glynn, in *Sulfate Minerals: Crystallography, Geochemistry, and Environmental Significance*, edited by C. N. Alpers, J. L. Jambor, and D. K. Nordstrom, Reviews in Mineralogy and Geochemistry No. 40 (Mineralogical Society of America and The Geochemical Society, 2000), Chap. 10, p. 481.